J|A|C|S ARTICLES

Published on Web 02/16/2009

Identification of Protonated Oxygenic Ligands of Ribonucleotide Reductase Intermediate X

Muralidharan Shanmugam,[†] Peter E. Doan,[†] Nicholas S. Lees,[†] JoAnne Stubbe,*[,‡] and Brian M. Hoffman*[,†]

Department of Chemistry, Northwestern University, Evanston, Illinois 60208-3113, and Department of Chemistry, Massachusetts Institute of Technology, Cambridge, Massachusetts 02139-4307

Received November 25, 2008; E-mail: stubbe@MIT.EDU; bmh@northwestern.edu

Abstract: We previously used a combination of continuous-wave (CW) and pulsed electron−nuclear double resonance (ENDOR) protocols to identify the types of protonated oxygen (OH_x) species and their disposition within the Fe^{III}/Fe^{IV} cluster of intermediate X, the direct precursor of the essential diferric-tyrosyl radical cofactor of the β2 subunit of *Escherichia coli* ribonucleotide reductase (RNR). We concluded that X contains the [$(H_xO)Fe^{III}OFe^{IV}$] fragment (T model), and does not contain a μ-hydroxo bridge. When combined with a subsequent ^{17}O ENDOR study of X prepared with $H_2{}^{17}O$ and with $^{17}O_2$, the results led us to suggest that this fragment is the entire inorganic core of X. This has been questioned by recent reports, but these reports do not themselves agree on the core of X. One concluded that X possesses a di-μ-oxo Fe^{III}/Fe^{IV} core plus a terminal (H_2O) bound to Fe^{III} [e.g., Han, W.-G.; Liu, T.; Lovell, T.; Noodleman, L. *J. Am. Chem. Soc.* **2005**, *127*, 15778−15790]. The other [Mitic, N.; Clay, M. D.; Saleh, L.; Bollinger, J. M.; Solomon, E. I. *J. Am. Chem. Soc.* **2007**, *129*, 9049−9065] concluded that X contains only a single oxo bridge and postulated the presence of an additional hydroxo bridge plus a terminal hydroxyl bound to Fe^{III}. In this report we take advantage of improvements in 35 GHz pulsed ENDOR performance to reexamine the protonation state of oxygenic ligands of the inorganic core of X by directly probing the exchangeable proton(s) with ^2H pulsed ENDOR spectroscopy. These ^2H ENDOR measurements confirm that X contains an Fe^{III}-bound terminal aqua ligand (H_xO), but the spectra contain none of the features that would be required for the proton of a bridging hydroxyl. Thus, we confirm that X contains a terminal aqua (most likely hydroxo) ligand to Fe^{III} in addition to one or two μ-oxo bridges but does not contain a μ-hydroxo bridge. The ^2H ENDOR measurements further demonstrate that this conclusion is applicable to both wild type and Y122F-β2 mutant, and in fact we detect no difference between the properties of protons on the terminal oxygens in the two variants; likewise, ^{14}N ENDOR measurements of histidyl ligands bound to Fe show no difference between the two variants.

Introduction

Diferrous non-heme iron proteins carry out a broad range of reactions, ranging from reversible O_2 binding to fatty acid desaturation and methane oxidation, and the factors that govern O_2 activation in such diverse reactions are of intense interest.[1−4] The β2 (R2) subunit of class 1a and 1b *Escherichia coli* ribonucleotide reductases (RNR) are such proteins. These RNRs catalyze the conversion of nucleoside diphosphates to deoxynucleoside diphosphates in reactions involving complex free radical chemistry.[5−7] The β2 subunits in their oxidized forms/states contain a non-heme diferric center adjacent to a tyrosyl radical ($Y^{\bullet}$)[8,9] that initiates the reduction process. The active diferric-$Y^{\bullet}$ cofactor is generated from the diferrous-Y center in a reaction with O_2 and an external reductant. This process has been studied by a number of time-resolved biophysical methods, including stopped-flow spectroscopy and rapid freeze−quench (RFQ) electron paramagnetic resonance (EPR), electron−nuclear double resonance (ENDOR), Mössbauer, magnetic cicrular dichroism (MCD), and extended X-ray absorption fine structure (EXAFS) spectroscopies.[10−16] A paramagnetic diiron intermediate designated X has been observed by all of these methods. X is one-electron oxidized relative to the resting diferric state of β2 and is catalytically competent to oxidize tyrosine 122 to $Y122^{\bullet}$.[17,18] RFQ Q-band ^{57}Fe ENDOR spectroscopy[19] established that the diiron center of X has an antiferromagnetically spin-coupled $Fe^{III}(S = {}^5/_2)/Fe^{IV}(S = 2)$ core with an $S = {}^1/_2$ ground state.

Efforts to assign the structure(s) of X have been influenced by crystallographically determined structures of β2 in the

[†] Northwestern University.
[‡] Massachusetts Institute of Technology.

(1) Eklund, H.; Uhlin, U.; Farnegardh, M.; Logan, D.; Nordlund, P. *Prog. Biophys. Mol. Biol.* **2001**, *77*, 177–268.
(2) Solomon, E. I.; Brunold, T. C.; Davis, M. I.; Kemsley, J. N.; Lee, S.-K.; Lehnert, N.; Neese, F.; Skulan, A. J.; Yang, Y.-S.; Zhou, J. *Chem. Rev.* **2000**, *100*, 235–349.
(3) Nordlund, P.; Eklund, H. *Curr. Opin. Struct. Biol.* **1995**, *5*, 758–766.
(4) Feig, A. L.; Lippard, S. J. *Chem. Rev.* **1994**, *94*, 759–805.
(5) Licht, S.; Stubbe, J. Mechanistic investigations of ribonucleotide reductases. In *Comprehensive Natural Product Chemistry, Vol. 5*; Poulter, C. D., Ed.; Elsevier Science: New York, 1999; pp 163−203.
(6) Stubbe, J.; Riggs-Gelasco, P. *Trends Biochem. Sci.* **1998**, *23*, 438–443.
(7) Stubbe, J.; van der Donk, W. A *Chem. Rev.* **1998**, *98*, 705–762.
(8) Atkin, C. L.; Thelander, L.; Reichard, P.; Lang, G. *J. Biol. Chem.* **1973**, *248*, 7464–7472.
(9) Larsson, A.; Sjöeberg, B. M. *EMBO J.* **1986**, *5*, 2037–2040.

10.1021/ja809223s CCC: $40.75

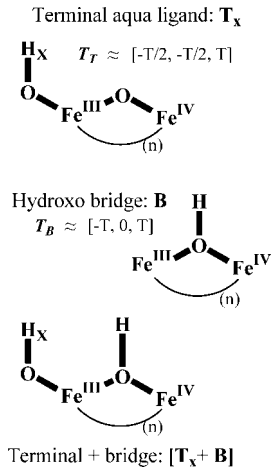

Figure 1. Alternate models for exogenous ligands to X, with the portions relevant to this study shown in boldface type. Top, oxo bridge plus terminal aqua ligand (T_x); middle, hydroxo bridge (B); bottom, terminal aqua plus bridge (T_x + B). Approximate characteristics of the ^{1,2}H cluster dipolar hyperfine tensors are indicated (eqs S1−S4 in Supporting Information).

diferrous state, of the tyrosyl radical reduced diferric state, and of several β2 mutants. In the diferrous state, the two irons are separated by 3.9 Å with Fe1, adjacent to the tyrosine 122 that is oxidized, being four-coordinate and Fe2 being five-coordinate.[20,21] In this state there are no ligands from the solvent; there are two glutamates, E115 and E238, that bridge the two iron centers in a μ-1,3 fashion. In addition, Fe1 is coordinated to H118 and D84, which also is H-bonded to Y122. During the conversion to the diferric cluster,[22,23] the iron centers move closer together (3.3 Å), E115 forms a single carboxylate bridge in a μ-1,3 fashion, and a single μ-oxo bridge is formed from O_2. Both iron ions become six-coordinate. Fe1 also is coordinated to H118, bidentate to D84, and to a water or hydroxide, whereas Fe2 is coordinated to H241, monodentate to E238 and E204 and a terminal water molecule. Thus, during the formation of active cofactor from the diferrous state, two terminal (H_xO) and μ-O have been incorporated.

The intermediate X formed in Y122F-β2 has been the focus of many studies because it accumulates to high levels, minimizing interference from other diiron species.[24] Studies of many other diiron proteins in different oxidation states indicate that the observed antiferromagnetic exchange-coupling between the Fe ions of X requires the presence of one or more oxo and/or hydroxo bridges. We previously used a combination of ^{1}H and ^{2}H continuous-wave (CW) and pulsed ENDOR protocols to identify the types of protonated oxygen (OH_x) species and their disposition relative to the ferric and ferryl ions of X.[12,25] We considered the possible presence, either separately or jointly, of an hydroxo bridge, which we denoted B, and a terminal aqua ligand (OH_x) bound to Fe^{III}, which we denoted T_x (Figure 1). Analysis of these data led us to conclude that the inorganic core

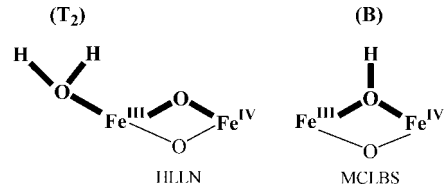

Figure 2. Inorganic cores of X models proposed by Noodleman and co-workers[27] (HLLN) and by Solomon and co-workers[10] (MCLBS), with the portions relevant to this study shown in boldface type.

of X contains such a terminal aqua ligand (OH_x) but not an hydroxo bridge. In addition, the data gave no evidence for an additional H_xO terminally bound to Fe^{IV} but did not rule it out. A subsequent ^{17}O ENDOR study of X, prepared either with $H_2{}^{17}O$ or with $^{17}O_2$, then led us to conclude that the [(H_xO)-$Fe^{III}OFe^{IV}$] fragment in fact is the complete inorganic core of X.[14] This interpretation has been questioned in several recent reports, but these reports do not themselves agree on the core of X. Detailed broken-symmetry DFT computations led Noodleman and co-workers[26,27] to conclude that X possesses a di-μ-oxo Fe^{III}/Fe^{IV} core plus a terminal (H_2O) bound to Fe^{III} (T_2, denoted HLLN, in Figure 2).[27] The Solomon group, using RFQ magnetic circular dichroism (MCD) measurements and TD-DFT calculations, instead concluded that there is only one oxo bridge and postulated the presence of an additional hydroxo bridge; the resulting μ-oxo/μ-hydroxo Fe^{III}/Fe^{IV} core is denoted MCLBS in Figure 2.[10] They further proposed a terminal hydroxyl bound to Fe^{III}.

In this report we take advantage of improvements in 35 GHz pulsed ENDOR performance to reexamine the protonation state of the oxygenic ligands of the inorganic core of X by *directly* probing the exchangeable proton(s) with ^{2}H pulsed ENDOR spectroscopy. We further use ^{2}H and ^{14}N ENDOR measurements to test whether the core structures of X in WT and Y122F-β2 variants are identical.

Materials and Methods

Samples. X in WT and Y122F β2 D_2O buffer was prepared by RFQ methods[12] and stored in liquid nitrogen since 1996. EPR and ENDOR spectroscopy (35 GHz) demonstrates that the signals are unchanged by this storage. The time points examined were 33 ms for X generated with WT-β2 and 610 and 1200 ms for X generated

(10) Mitic, N.; Clay, M. D.; Saleh, L.; Bollinger, J. M.; Solomon, E. I. *J. Am. Chem. Soc.* **2007**, *129*, 9049–9065.
(11) Riggs-Gelasco, P. J.; Shu, L.; Chen, S.; Burdi, D.; Huynh, B. H.; Que, L., Jr.; Stubbe, J. *J. Am. Chem. Soc.* **1998**, *120*, 849–860.
(12) Willems, J.-P.; Lee, H.-I.; Burdi, D.; Doan, P. E.; Stubbe, J.; Hoffman, B. M. *J. Am. Chem. Soc.* **1997**, *119*, 9816–9824.
(13) Burdi, D.; Sturgeon, B. E.; Tong, W. H.; Stubbe, J.; Hoffman, B. M. *J. Am. Chem. Soc.* **1996**, *118*, 281–282.
(14) Burdi, D.; Willems, J.; Riggs-Gelasco, P.; Antholine, W.; Stubbe, J.; Hoffman, B. *J. Am. Chem. Soc.* **1998**, *120*, 12910–12919.
(15) Ravi, N.; Bollinger, J. M., Jr.; Huynh, B. H.; Edmondson, D. E.; Stubbe, J. *J. Am. Chem. Soc.* **1994**, *116*, 8007–8014.
(16) Bollinger, J. M., Jr.; Tong, W. H.; Ravi, N.; Huynh, B. H.; Edmondson, D. E.; Stubbe, J. *J. Am. Chem. Soc.* **1994**, *116*, 8024–8032.
(17) Bollinger, J. M., Jr.; Edmondson, D. E.; Huynh, B. H.; Filley, J.; Norton, J. R.; Stubbe, J. *Science* **1991**, *253*, 292–298.
(18) Bollinger, J. M., Jr.; Tong, W. H.; Ravi, N.; Huynh, B. H.; Edmondson, D. E.; Stubbe, J. *J. Am. Chem. Soc.* **1994**, *116*, 8015–8023.
(19) Sturgeon, B. E.; Burdi, D.; Chen, S.; Huynh, B. H.; Edmondson, D. E.; Stubbe, J.; Hoffman, B. M. *J. Am. Chem. Soc.* **1996**, *118*, 7551–7557.
(20) Logan, D. T.; Su, X. D.; Aberg, A.; Regnstrom, K.; Hajdu, J.; Eklund, H.; Nordlund, P. *Structure* **1996**, *4*, 1053–1064.
(21) Wei, P.-p.; Skulan, A. J.; Mitic, N.; Yang, Y.-S.; Saleh, L.; Bollinger, J. M., Jr.; Solomon, E. I. *J. Am. Chem. Soc.* **2004**, *126*, 3777–3788.
(22) Nordlund, P.; Eklund, H. *J. Mol. Biol.* **1993**, *232*, 123–164.
(23) Nordlund, P.; Aberg, A.; Eklund, H. *Biochemistry Soc. Trans.* **1993**, *21*, 735–738.
(24) Tong, W.; Burdi, D.; Riggs-Gelasco, P.; Chen, S.; Edmondson, D.; Huynh, B. H.; Stubbe, J.; Han, S.; Arvai, A.; Tainer, J. *Biochemistry* **1998**, *37*, 5840–5848.
(25) Willems, J.-P.; Lee, H.-I.; Burdi, D.; Doan, P. E.; Stubbe, J.; Hoffman, B. M. In *ACS Advances in Chemistry*; Solomon, E., Hodgson, K., Eds.; American Chemical Society: Washington, DC, 1998; pp 2−15.
(26) Han, W.-G.; Liu, T.; Lovell, T.; Noodleman, L. *Inorg. Chem.* **2006**, *45*, 8533–8542.
(27) Han, W.-G.; Liu, T.; Lovell, T.; Noodleman, L. *J. Am. Chem. Soc.* **2005**, *127*, 15778–15790.

with Y122F-β2. In both cases, the amount of X is maximized at these times. Comparison of the results for the two variants thus provides insight into the role of the phenolic hydroxyl group of Y122 on the properties of X.

ENDOR Spectroscopy. Previous studies of X employed 35 GHz CW and pulsed ^{1,2}H ENDOR spectroscopy of exchangeable hydrogenic species associated with X; in this report we discuss only pulsed ^{2}H measurements. The recent upgrade to the 35 GHz pulsed-ENDOR spectrometer[28] employed in this study has been described.[29] In the text we present only ^{2}H ENDOR spectra that were collected by the Davies (t_p-T-$t_{p/2}$-τ-t_p-τ-echo) ENDOR sequence (radio frequency, rf, applied during interval T); in Supporting Information we present both Davies and Mims (t_p-τ-t_p-T-t_p-τ-echo)[30] pulsed ENDOR measurements. In all measurements, frequency values within the radio frequency range chosen for the spectrum were accessed randomly (stochastic ENDOR). Signal averaging was accomplished by collecting multiples of such spectra rather than by multiple acquisitions at each frequency within a spectrum.[31] The enhanced signal/noise ratio (S/N) provided by this single-point stochastic ENDOR approach has enabled the reassessment described herein.

The enhanced S/N had one unanticipated consequence. While samples prepared in H_2O buffer previously had flat backgrounds in the ^{2}H ENDOR region, they now reveal broad features associated with ^{14}N that persist in the ^{2}H spectra for enzyme in D_2O. These features reproduce *precisely*, so many of the ^{2}H ENDOR spectra presented here have had the background subtracted, as noted in the figure captions. To demonstrate that this procedure is totally benign, we present the corresponding primary data, foreground and background together, in Figure S1 in Supporting Information.

The Davies sequence intrinsically introduces a modulation of the ENDOR intensity that varies with the hyperfine coupling, A, and must be accounted for in simulations. The Davies ENDOR response, R, is jointly dependent on the hyperfine coupling, A, and the length of the microwave pulse, t_p, through the selectivity factor, η:

$$R = R_0\left(\frac{1.4\eta}{0.7^2+\eta^2}\right) \qquad \eta = At_p \tag{1}$$

where R_0 is the maximum ENDOR response.[30] For fixed t_p, this function suppresses the ENDOR response as $A \rightarrow 0$, it rises to a maximum at $At_p = 0.7$, and then it falls to 0. As a result, the ^{2}H ENDOR spectra of X displayed here do not show features from the weakly coupled exchangeable protons. The Mims response shows periodic maxima and minima as function of $\eta' = A\tau$, with the first maximum at $\eta' = 0.5$.

A deuteron ENDOR signal for a single molecular orientation consists of a doublet centered at the Larmor frequency, ν_D, and split by the orientation-dependent hyperfine coupling A; spectra in this paper are plotted as $\Delta\nu = \nu - \nu_D$. In this report, a ^{2}H ENDOR signal consists of a doublet centered at ν_D and split by A_D; the additional splitting from the nuclear quadrupole interaction expected for the ($I = 1$) ^{2}H nucleus is not resolved for the strongly coupled deuteron signals discussed here. The Larmor frequency and hyperfine constants of protons and deuterons are related by the equation: $\nu_H/\nu_D = A_H/A_D = g_H/g_D = 6.5$. As discussed in detail,[32−34] for a frozen solution sample, the determination of the full hyperfine tensor (and quadrupole tensor) of an interacting nucleus is achieved by obtaining a 2-D set of orientation-selective ENDOR spectra collected at multiple fields across the EPR envelope and comparing this set with simulated 2-D patterns. The ENDOR simulations were performed with the program Gensim, an enhanced version of the simulation program GENDOR.[32] The Davies and Mims response factors have a major influence on the observed ENDOR response and are incorporated into Gensim.

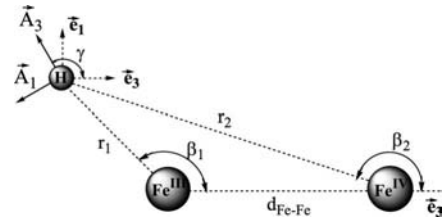

Figure 3. Geometry used in calculation of cluster dipolar interaction tensor **T** (eqs S1−S4 in Supporting Information).

^{1,2}H Hyperfine Interactions of Protonated Oxygenic Ligands. Our work[12,35] has shown that the hyperfine tensor for a proton of a bridge or a terminal aqua (water/hydroxo) ligand is dominated by the through-space dipolar contribution, **T**, arising from with interactions with the Fe ions of the diiron center of X ($\mathbf{A} = \mathbf{T} + a_{iso}\mathbf{U}$, where $\mathbf{U}$ = unit matrix). Equations have been derived to calculate the observed dipolar coupling tensor for a nucleus in an arbitrary position relative to the two Fe ions of an $S = {}^1/_2$ spin-coupled [$Fe^{III}(S = {}^5/_2)$−$Fe^{IV}(S = 2)$] diiron center;[12] these equations are reproduced in Supporting Information. The principal values are functions of the cluster's metrical parameters as defined in Supporting Information; the component T_2 lies normal to the Fe(H)Fe plane and **T**/**A** are rotated about the T_2/A_2 direction by the angle γ, shown in Figure 3 (eq S3, Supporting Information), which also is determined by the structure. The isotropic coupling, a_{iso}, of such protons is small or even negligible.

For a terminal water (or hydroxide) the dipole interaction tensor (**T**) with the liganding iron ion dominates the ^{1,2}H hyperfine interaction tensor (**A**). It is approximately axial, $\mathbf{T} \sim [-{}^1/_2T, -{}^1/_2T, T]$, with the T_3 axis lying close to the Fe−H vector; $T \sim ({}^7/_3)g\beta g_n\beta_n/r_1{}^3$ when the ligand is bound to the ferric ion but $T \sim (-{}^4/_3)g\beta g_n\beta_n/r_2{}^3$ when it is bound to the ferryl ion. In contrast, a proton of a bridging hydroxide interacts strongly with both Fe ions and is characterized by a nearly rhombic dipolar tensor, $\mathbf{T} \sim [-T, 0, T]$, with the rotation of **T** about the A_2 direction such that A_1 and A_3 do not point toward a specific atom.

A model-free determination of **A** through simulations of the experimental 2-D ENDOR field-frequency pattern gives the principal values of **A** and its orientation within the **g** tensor reference frame. As discussed in Supporting Information, if the orientation of **A** is determined by the through-space dipolar interaction with the cluster Fe spins, **T**, then the orientation of **A** in the molecular (**e**) frame is determined (Figure 3) and through this the experimentally determined orientation of **g** relative to the **e** frame can be derived.[36]

Results and Discussion

EPR Spectra of X. The EPR spectra of X appear isotropic when collected at X-band, but at 35 GHz they show moderately well-resolved features that permit determination of the **g**-tensor components. Most importantly here, this allows us to collect orientation-selective 2-D field-frequency patterns of ENDOR

(28) Davoust, C. E.; Doan, P. E.; Hoffman, B. M. *J. Magn. Reson.* **1996**, *119*, 38–44.
(29) Zipse, H.; Artin, E.; Wnuk, S.; Lohman, G. J. S.; Martino, D.; Griffin, R. G.; Kacprzak, S.; Kaupp, M.; Hoffman, B.; Bennati, M.; Stubbe, J.; Lees, N. *J. Am. Chem. Soc.* **2008** (in press).
(30) Fan, C.; Doan, P. E.; Davoust, C. E.; Hoffman, B. M. *J. Magn. Reson.* **1992**, *98*, 62–72.
(31) Epel, B.; Arieli, D.; Baute, D.; Goldfarb, D. *J. Magn. Reson.* **2003**, *164*, 78–83.
(32) Hoffman, B. M.; DeRose, V. J.; Doan, P. E.; Gurbiel, R. J.; Houseman, A. L. P.; Telser, J. *Biol. Magn. Reson* **1993**, *13*, 151–218.
(33) Hoffman, B. M. *Acc. Chem. Res.* **2003**, *36*, 522–529.
(34) Hoffman, B. *Proc. Natl. Acad. Sci. U.S.A.* **2003**, *100*, 3575–3578.
(35) DeRose, V. J.; Liu, K. E.; Lippard, S. J.; Hoffman, B. M. *J. Am. Chem. Soc.* **1996**, *118*, 121–134.
(36) Lees, N. S.; McNaughton, R. L.; Gregory, W. V.; Vela, J.; Holland, P. L.; Hoffman, B. M. *J. Am. Chem. Soc.* **2008**, *130*, 546–555.

spectra taken at multiple fields across the EPR envelope; their analysis yields the hyperfine interaction tensors of coupled nuclei.

Alternative Models for Identity of the Strongly Coupled Exchangeable ^{1,2}H of X. Our previous studies[12,13] revealed ^{1,2}H ENDOR signals from strongly coupled exchangeable proton(s) and considered their possible association with a terminal aqua ligand (OH_x) (Figure 1, top), an hydroxo bridge (Figure 1, middle), or both (Figure 1, bottom). To distinguish among these, we optimized simulations of a 2-D field-frequency pattern composed of ^{1,2}H ENDOR spectra taken at multiple fields across the EPR envelope of X under the assumption either of the presence of a bridging hydroxyl (B model) or of an aqua ligand terminally bound to Fe^{III} (T model), each with a net dipolar hyperfine coupling tensor, **T**, to the spin-coupled iron ions given by eqs S1−S4 in Supporting Information.

In our earlier work, the geometric parameters that define the dipolar coupling calculations for the B and T_x models were chosen to best reflect the EXAFS data then available, in keeping with general bonding principles. These were used in conjunction with eqs S1−S4 in Supporting Information to generate 2-D patterns of ^{1,2}H ENDOR spectra that optimized the agreement with experiment by constraining the calculated spectra at g_1 and g_3 to match experiment. Although this constraint guaranteed a qualitative similarity between the predicted 2-D patterns of the B and T models, key differences between them, primarily in the spectra between g_2 and g_3, led us to the T model we reported. This model required the assumption that the terminal aqua ligand had two slightly different ^{2}H, reflecting the presence of either of a terminal H_2O or a 2-fold disordered hydroxyl.

In the present study we have the advantage of also being able to predict electron−nuclear dipolar interactions for B models based on recent DFT-determined structural models of the core of X. MCLBS reported their preferred structure, a B model. HLLN reported as their preferred model a T_2 structure of X (Figure 2, HLLN) that has a terminal H_2O but not an hydroxo bridge (for clarity, denoted T_2). However they also reported the structure of a T_2 + B model (Figure 1, bottom, $x = 2$), which has both types of proton, denoted here as HLLN(2). As discussed below, we employed the metrical parameters of these two structures as input in determining the principal values of **T** (eqs S1−S4 in Supporting Information) for both types of proton; these are presented in Table 1. In addition, when the two types of proton are assumed to be present simultaneously, use of the HLLN(2) structure allowed us to determine the orientation of **g** in the molecular (**e**) coordinate frame (Figure 3). We emphasize, however, that the calculated values are insensitive to variations to the structure of the inorganic core of X.

Deuteron ENDOR of Intermediate X. Our previous study described the basic features of the ^{1,2}H ENDOR response of X. It exhibits strongly coupled, exchangeable ^{1,2}H signals, $8 \leq A(^1H) \leq 20$ MHz, from protonated oxygenic ligands, plus numerous signals from more weakly coupled ^{1,2}H, $A(^1H) \leq 8$ MHz, some of which were exchangeable. In the study of the strongly coupled ^{1,2}H, limitations in S/N compelled us to combine ^{1,2}H CW and pulsed measurements of X to obtain the 2-D field-frequency ^{1,2}H ENDOR patterns for the protonated oxygenic ligands that are used to derive hyperfine tensors. With the improved S/N now available from the pulsed spectrometer, we have collected full 2-D Davies pulsed ^{2}H ENDOR patterns for these exchangeable deuteron(s) for X quenched in D_2O buffer.

Table 1. Metrical and ^{2}H Spin Hamiltonian Parameters Used To Calculate[a] the 2-D ENDOR Patterns Displayed in Figure 4a,b

	terminal OH_x			bridging OH		
	experimental		calculated[c]	optimized		calculated[d]
	$\mathbf{A}^{ex}$ [b]	$\mathbf{T}^{ex}$	$\mathbf{T}_T$	$\mathbf{A}_B^0$ [b]	$\mathbf{T}_B^0$	$\mathbf{T}_B$
A_1/T_1 (MHz)	−1.55	−1.717	−1.718	−3.031	−2.764	−2.762
A_2/T_2 (MHz)	−1.15	−1.317	−1.316	−0.948	−0.681	−0.681
A_3/T_3 (MHz)	3.2	3.033	3.034	3.179	3.446	3.443
$\lambda = (T_2 - T_1)/T_3$		0.132	0.132		0.604	0.604
A_{iso} (MHz)	0.167			−0.267		
r_1 (Å)			2.625			2.67
β (deg)			94.5			59.3
γ (deg)			90.0			50.1
d_{FeFe} (Å)			2.84			2.817

[a] Simulations employed $\mathbf{g} = [g_1, g_2, g_3] = [2.0056, 1.9977, 1.993]$. Quadrupole splitting for ^{2}H ($I = 1$) is not resolved; their inclusion had no effect on simulations, so they were not incorporated. [b] Euler angles for $\mathbf{A}^{ex}$ are $\alpha = 10.5°$, $\beta = 72.0°$, and $\gamma = 0.0°$. Euler angles for $\mathbf{A}_B$ are $\alpha = 0.0°$, $\beta = 115.0°$, and $\gamma = 75.0°$. For definition of angles, see ref 32. [c] The calculation was optimized from structure HLLN(2) by taking an approximately average position of protons 1 and 2, for which **T** best agrees with experiment. [d] Calculated from structure MCLBS with slight alterations of metrical parameters.

Experiments were performed on samples of X(WT) (Figures 4, 5, and S1 in Supporting Information) and X(Y122F) (Figures S2B and S3 in Supporting Information) freeze-quenched so that the time delays after mixing are long compared to the half-time for formation of X. The ^{2}H ENDOR response appears in a radio frequency region that contains signals from ^{14}N of histidine bound to the Fe ions. To enhance the ability to compare the ^{2}H ENDOR experiment and simulation, the spectra of X(WT) in Figure 4 have had the corresponding background, collected from a sample prepared in H_2O buffer, digitally subtracted. As can be seen in Figure S1 (Supporting Information), the ^{14}N features are faithfully reproduced in foreground and background spectra, and the subtraction procedure introduces no distortions. Figure S2A (Supporting Information) shows that the 2-D ^{2}H ENDOR patterns of X(WT) and X(Y122F) are indistinguishable, indicating that neither the mutation nor the quench delay influences this property of X.

Terminal (T_x) versus Bridging (B) OH. Model-free simulation of the 2-D ^{2}H ENDOR patterns for X in D_2O yielded spectra that reproduce experiment with superb fidelity (Figure 4a). These simulations employed only a single (type of) contributing deuteron whose hyperfine tensor, $\mathbf{A}_T^{ex}$ (Table 1), has the axial character predicted for the T model of a terminal aqua ligand (Figure 1, top). The overall description matches rather well with that reported previously. However, the fit of the improved data to a model with a single type of terminal deuteron now implies that if this signal represents two deuterons, they must be very nearly magnetically equivalent. The principal values of the experimental dipolar interaction tensor, $\mathbf{T}_T^{ex}$, match well with those calculated with the dipolar equations (eqs S1−S4 in Supporting Information) for a terminal [H_xO−Fe^{III}] of the X diiron center. The optimized location of ^{2}H relative to the iron ions ($\beta 1$, $r1$) (Tables 1 and S1 in Supporting Information) is roughly bracketed by those of the two protons of the terminal H_2O of HLLN2 (Figure 6, Table S1 in Supporting Information). However, note that a D_2O with this orientation would give an ENDOR pattern in which the signals from the two deuterons are resolved, contrary to experiment.

To test whether the experiments could be comparably well-described by the B model, we generated an optimized ^{2}H hyperfine tensor, $\mathbf{A}_B^o$ (Table 1), for the hydroxo bridge as

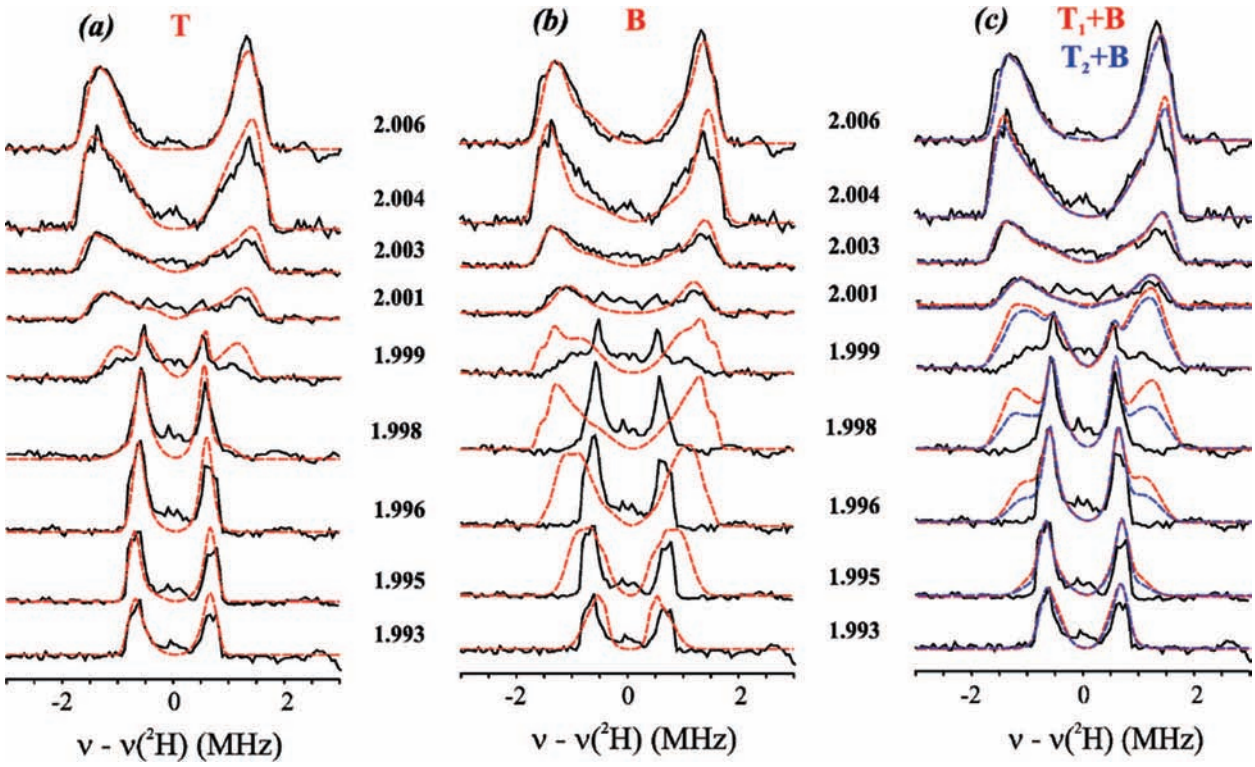

Figure 4. Experimental 2-D field-frequency plots of Davies ^{2}H ENDOR spectra of X(WT) in D_2O. Red and blue curves are simulations with the three models considered here (Figure 1, see text and Table 1): (a) T; (b) B; (c) T_x + B, considered here. Conditions: π-pulse length = 200 ns, τ = 600 ns, repetition time = 50 ms, MW frequency = 34.826 GHz, T = 2 K. All spectra are centered at the ^{2}H nuclear Larmor frequency. Backgrounds have been subtracted from experimental spectra as discussed (see Materials and Methods and Supporting Information.). (a) Experiment with T proton simulations overlaid. Simulation parameters (determined as described in text): $\mathbf{g} = [g_1 = 2.0056, g_2 = 1.9977, g_3 = 1.993]$, $\mathbf{A} = [A_1 = -1.55, A_2 = -1.15, A_3 = 3.2]$ MHz (Euler angles $\alpha = 10.5°$, $\beta = 72°$, $\gamma = 0$), line widths used = 0.09 (minimum) to 0.25 (maximum) MHz. (b) Experiment with simulations of the B proton model, optimized by including a_{iso}. Spin Hamiltonian parameters for the bridging hydroxide (optimized); $\mathbf{g} = [g_1 = 2.0056, g_2 = 1.9977, g_3 = 1.993]$, $\mathbf{A} = [A_1 = -3.031, A_2 = -0.948, A_3 = 3.179]$ MHz (Euler angles $\alpha = 0.0°$, $\beta = 115.0°$, $\gamma = 75.0°$), linewidths range from 0.08 (minimum) to 0.25 (maximum) MHz. (c) Experiment with simulations of T_x + B models: $x = 1$ (red), $x = 2$ (blue). For parameters for simulations of terminal and optimized bridging hydroxides, see panels A and B and Table 1. For $x = 1$, the intensities of the T and B deuteron signals were added and the result was scaled to the maximum of the experiment; for $x = 2$, twice the T intensity was added to the B intensity before scaling.

follows. We used eqs S1−S4 (Supporting Information) to calculate $\mathbf{T}_B$ for the bridging hydroxyl of the MCLBS and HLLN2 structures and performed simulations as the orientation of each was varied with respect to **g**. The best results were obtained when $\mathbf{A}_B{}^o$ included the dipolar interaction similar to that of the MCLBS hydroxyl plus a small isotropic component (Table 1). These optimized simulations are overlaid on experiment in Figure 4b. As in our previous study, these simulations based on an optimized B model for the exchangeable deuteron reproduce the spectra at the edges of the EPR envelope (g_1 and g_3) but are poor at fields away from the edges, particularly at fields between g_2 and g_3, We thus confirm the previous conclusion that the observed ^{1,2}H signals cannot be described by assuming that the only protonated oxygenic ligand in the core of X is an hydroxo bridge.

As the simulations of the pulsed ^{2}H ENDOR data in Figure 4a involve a single type of ^{2}H associated with a terminal aqua ligand, they are most simply assigned to a terminal hydroxyl with a single *major* orientation. The requirement of systematic variations of the ENDOR line width further suggests a modest distribution in position of the deuteron. We cannot exclude the possibility of a H_2O ligand whose two protons accidentally are equivalent and indistinguishable within the resolution of our spectra, but an hydroxyl could act as a proton acceptor during oxidations of Y122 and hence seems more likely to us. The recent DFT study of HLLN inferred the presence of a water ligand to Fe^{III}, while the study of MCLBS does not address the issue.

T_x + B, Terminal plus Bridging? Could X contain *both* T and B protons, the T_x + B model of Figure 1, as might be inferred from the MCLBS study? In our earlier study we had considered this question by looking for ^{1,2}H ENDOR intensity that is not accounted for by the T model. A comparison of simulations for the T and B models (Figure 1) suggested that the optimal fields to look for intensity from a B deuteron would be in the field range from $\sim g_2$ to g_3, where the T deuteron(s) had their smallest splitting and calculated B spectra were appreciably broader. Although we recognized that the broader signals from a B deuteron would presumably be less intense than the narrower signals from the T deuteron(s), no additional signals were detected in spectra where extensive signal averaging had produced good signal/noise ratios. We had thus concluded that there is no hydroxo bridge.

The improved data reported here has allowed us to reexamine this possibility, and in doing so we have adopted a more "directed" approach. In the previous study we were forced to look for signals from a B deuteron without knowing what fields and frequencies were best to find them or how intense they might be if present. The present study removes this limitation. We have used multiple approaches to calculate the spectra to

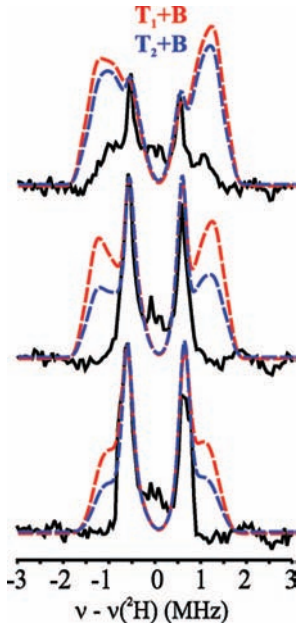

Figure 5. Decisive comparisons between experimental ^{2}H ENDOR responses for X(WT) and simulations for the T_x + B models, as described in Figure 4: g = 1.999 (top), 1.998 (middle), and 1.996 (bottom).

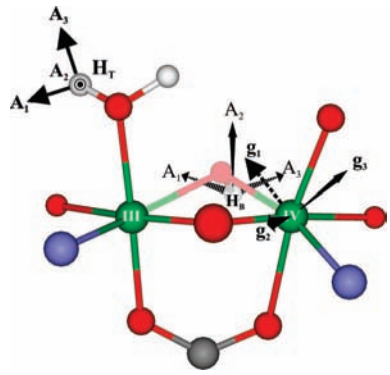

Figure 6. Orientation of $\mathbf{A}_T$, $\mathbf{T}_B/\mathbf{A}_B$ for H^T of the hypothetical HLLN(2) model of X, along with the orientation of **g** in the molecular frame as determined from $\mathbf{A}_T$ and experimental simulation parameters (see Supporting Information). $\mathbf{T}_T$ is not shown for the other terminal proton.

be expected if both T and B deuterons were present and have compared them with experiment.

To predict the ENDOR response for a hypothetical X with both T and B deuterons (T_x + B, Figure 1) we assumed the presence of either one or two T deuterons described by $\mathbf{A}_T^{ex}$ (Table 1), namely, either a terminal hydroxo (T_1) or a terminal water (T_2 in Figure 2) that has two magnetically equivalent deuterons. As the most straightforward approach to describing a B deuteron, we assigned to B the hyperfine tensor $\mathbf{A}_B^o$, as defined above (Table 1) and calculated the 2-D field-frequency patterns expected if both T and B deuterons were present (Figure 4c). So as not to overestimate the ease of detecting a signal from B, we used for the T deuterons the same field-dependent line width as in Figure 4a, but at all fields used a line width for B that equaled the largest line width used for the T deuteron(s) at any field (the value near g_1), rather than the optimized B line widths used in Figure 4b. Figure 4c displays the resulting composite 2-D ^{2}H ENDOR pattern calculated for models with both x = 1 and x = 2 protons on the terminal OH_x along with the B deuteron (T_1 + B and T_2 + B models, respectively), each overlaid onto the experimental ^{2}H ENDOR pattern for X(WT); Figure 5 separately presents the experimental and calculated spectra for fields at which the presence of a B deuteron would be most obvious. It is obvious that none of the intensity predicted for a B deuteron is present in the experimental spectra.

As an alternate means of simulating the T_1 or T_2 + B model of X, we employed the HLLN2 structure for X (Figure 6) in a recently developed simulation approach.[36] HLLN2 incorporates H_2O terminally bound to Fe^{III} and an hydroxo bridge that carries the B proton, as well as an oxo bridge. To calculate the ^{2}H ENDOR spectra expected for this B proton, we assigned the experimentally determined T-proton hyperfine tensor, $\mathbf{A}_T^{ex}$, first to one of the deuterons of the terminal H_2O of HLLN2 (eg., H_T of Figure 6) and then to the other, in each case taking $\mathbf{A}_T^{ex}$ as coaxial with $\mathbf{T}_T$ calculated with eqs S1−S4 in Supporting Information; then we used the experimentally determined orientation of $\mathbf{A}_T^{ex}$ relative to **g** to fix the orientation of **g** in the molecular frame (Figure 6). Once this was known, we could use eqs S1−S4 (Supporting Information) to calculate the dipolar interaction for the B deuteron, $\mathbf{T}_B$, from the HLLN(2) structure and to compute the 2-D patterns of ^{2}H ENDOR spectra to be expected if both types of deuteron were present

In all these computations, as shown in Figures S4 and S5 in Supporting Information, the simulations predict additional ^{2}H ENDOR intensity associated with B that would be even more obvious and readily detected than if a bridging proton had the optimized hyperfine tensor, $\mathbf{A}^B$ (Figure 5). *No such intensity is seen in the experiment.*

A technical observation about the experiments and simulations also is of interest. Each of the ENDOR simulations of Figures 4 and 5 is a statistical/geometric sum of the contributions from the subset of orientations that contributes to the EPR spectrum at the g-value of observation.[32] In such a simulation, the integrated ENDOR intensity of a T and B deuteron would be equal. As the B spectrum is broader and is calculated with a greater component ENDOR line width, if statistical/geometric considerations were all that was important for determining intensities, the relative intensities of features associated exclusively with B would be much less than those of the T proton, making the detection of B harder than it is seen to be in Figures 4c and 5. However, the sharp T doublet has a smaller hyperfine coupling and is suppressed to a greater degree by the Davies ENDOR response (eq 1). Thus, curiously, while the suppression effect reduces the overall S/N of the spectra, it helps enable us to state with confidence that X does not contain a B proton in addition to the T proton(s).

In short, the absence in the spectra of *any* of the unexplained features that would be required for the proton of a μ-(OH) bridge rules out the presence of such a moiety, either alone or in addition to the Fe^{III}-bound terminal aqua ligand (H_xO): only the latter is present (T_x model of Figure 1), in agreement with our proposal of over a decade ago.[12]

The conclusion by HLLN (Figure 2) that X does not have an hydroxo bridge agrees with our earlier proposal and current conclusion, whereas the report of MCLBS instead postulated the presence of an hydroxo bridge. As all three proposals differ in some regard, some critical comments are in order. *First*, and most important, ENDOR measurements *directly* interrogate the protons associated with the oxygenic ligands of X, and are not influenced by other enzyme forms that might be present. Thus in our view they must take priority over other approaches in this question of protonation state. *Second*, HLLN and MCLBS based their proposals on different computational treatments of

two or more spectroscopic studies. Solomon and co-workers used TD-DFT computations in interpreting their RFQ-MCD measurements as requiring one oxo bridge and being incompatible with two, and postulated the presence of an hydroxo bridge as a means of enforcing the short Fe–Fe distance inferred from EXAFS measurements (~2.5 Å). HLLN used broken-symmetry DFT computations with a more complete model of the diiron center. They explored multiple possible models for the core and judged the bis-μ-oxo structure as giving both a short Fe–Fe distance and better agreement with spectroscopic measurements, including the MCLBS data. *Last*, it may be that additional tests of the new sample preparation procedure of MCLBS, which differ from that used in all previous RFQ studies,[12−15,19,37,38] would be instructive. The MCD study involved freeze-quenching by spraying into liquid nitrogen, rather than liquid pentane, which gives longer freezing times. Also, high concentrations of glycerol were added at −30 °C as a glassing agent subsequent to freeze-quenching. Although MCLBS carried out 9 GHz EPR experiments to test whether X prepared in their procedure is the same as in the samples prepared previously, the signal of X appears isotropic at X band and is not a particularly sensitive test for subtle structural differences that might occur.

Other ^{1,2}H ENDOR Signals and the Possibility of a H_xO Bound to Fe^{IV}. In our earlier work we observed nonexchangeable ^{1}H ENDOR signals from the protein matrix− to be associated with ligands to the diiron center and nearby amino acids. In addition, we saw weakly coupled exchangeable ^{2}H signals, presumably from histidine−imidazole, amino/amido N−H, etc. We found no evidence for exchangeable ^{2}H ENDOR signals that would be associated with H_xO bound to Fe^{IV}. Combining this with the subsequent failure to find a ^{17}O signal from such a species, we concluded that none was present. In the present study we also reconsidered the possibility of H_xO bound to Fe^{IV}. Such a proton is predicted (eqs S1−S4, Supporting Information) to have a roughly rhombic dipolar tensor with maximum ^{2}H tensor components of ~2 MHz. To test for signals from such a proton we collected both ^{2}H Mims (Figure S6 in Supporting Information) and ^{2}H "soft" (t_p = 200 ns) Davies pulsed ENDOR spectra (Figures 4 and S1, Supporting Information), but neither gave any evidence for ^{1,2}H ENDOR intensity for such a proton. Thus, the present effort is consistent with our earlier conclusion, as well as with the computations of HLLN.

Possible Effects of the Y122F Mutation. The 2-D patterns of ^{2}H ENDOR spectra of X(WT) and X(Y122F) are identical, within error (Figure S2A, Supporting Information), as are the hyperfine tensors determined by simulating those patterns (Table 1; Figures 4a and S2B, Supporting Information). To search for other possible influences of the mutation we collected 2-D field-frequency plots of ^{14}N ENDOR spectra for X(WT) and X(Y122F). Figure S3 (Supporting Information) shows that these plots for the two likewise are indistinguishable.

Conclusions

In this report we take advantage of improvements in 35 GHz pulsed ENDOR signal/noise to reexamine the protonation state of the oxygenic ligands of inorganic core of X directly by probing the exchangeable protons of X(WT) and X(Y122F) with ^{2}H pulsed-ENDOR spectroscopy. The 2-D pattern of Q-band ^{2}H ENDOR spectra collected for the strongly coupled exchangeable proton(s) of X(WT and Y122F) are indistinguishable (Figure S2A, Supporting Information), and the same is true for ^{14}N ENDOR measurements of histidyl ligands bound to Fe, together indicating that the Y122F mutation does not alter the properties of X.

Simulations of the ^{2}H 2-D field-frequency ENDOR patterns (Figures 4a and S2B in Supporting Information) of X show that the exchangeable proton/deuteron signals belong to the proton of a terminal aqua ligand bound to Fe^{III} (Figure 1, T_x model), likely an hydroxo ligand. Simulations based on both the B and T_x + B models (Figure 4b,c and Figures S4 and S5 in Supporting Information) completely fail to reproduce the data, demonstrating that X does *not* contain an hydroxo bridge, either alone (B) or with a terminal aqua ligand (T_x + B). The measurements further support the conclusion that there is no aqua ligand bound to Fe^{IV}. Overall, these findings thus establish that the inorganic core of X does not include a μ-hydroxo bridge and does contain the [$(H_xO)Fe^{III}OFe^{IV}$] fragment that defines the T_x model (Figure 1, top), likely with $x = 1$. The enhanced 35 GHz pulsed ENDOR capabilities will further permit us to revisit the question of whether X contains a second oxo bridge.

Acknowledgment. We express our gratitude toward C. E. Davoust for his technical support and to the National Institutes of Health [Grants HL 13531 (B.M.H.) and GM 29595 (J.S.)]. The samples studied here were prepared by Dr. Doug Burdi.

Supporting Information Available: Calculation of dipolar interactions (eqs S1−S4), Figures S1−S6, and Tables S1 and S2. This material is available free of charge via the Internet at http://pubs.acs.org.

JA809223S

(37) van der Donk, W. A.; Stubbe, J.; Gerfen, G. J.; Bellew, B. F.; Griffin, R. G. *J. Am. Chem. Soc.* **1995**, *117*, 8908–8916.
(38) Bollinger, J. M., Jr.; Tong, W. H.; Ravi, N.; Huynh, B. H.; Edmondson, D. E.; Stubbe, J. In *Methods in Enzymology*; Klinman, J. P., Ed.; Academic Press: New York, 1995; p 258.
(39) Additional solutions are closely related and need not be considered separately.